

# Interaction of amorphous Si and crystalline Al thin films during low-temperature annealing in vacuum

Y.H. Zhao, J.Y. Wang\*, E.J. Mittemeijer

Max Planck Institute for Metals Research, Heisenbergstr. 3, D-70569 Stuttgart, Germany

## Abstract

A Si(150 nm, amorphous)/Al(50 nm, crystalline; {111} fiber textured) bilayer was prepared by magnetron sputter deposition and isothermally annealed at 250 °C for 60 min in a vacuum of  $2.01 \times 10^{-4}$  Pa. X-ray diffraction, Auger electron spectroscopy and focused-ion beam microscopical techniques were used for compositional and microstructural analyses. A major observation was that after the annealing the Al and Si sublayers had exchanged their location in the bilayer; i.e. the Si layer was adjacent to the substrate after annealing. The amorphous Si layer had crystallized into a {111} textured polycrystal. The Al layer, now adjacent to the surface, had formed a uniformly net-shaped layer. Upon this rearrangement, the already initially present Al {111} fibre texture had become stronger, the Al crystallites had grown laterally and the microstrain in the Al layer had relaxed. The macrostress parallel to the surface in the Al layer had changed from the initially compressive value of  $-139$  MPa to the tensile value of  $+182$  MPa after annealing. An extensive analysis of thermodynamic driving forces for the transformation was made. © 2003 Elsevier Science B.V. All rights reserved.

**Keywords:** Crystallization and layer exchange; Crystallite size; Microstrain; Texture and macrostress

## 1. Introduction

In the last decades, interdiffusion and/or reactions between semiconductor (e.g. Si, Ge, etc.) and metal (Al, Ni, Cu, Ag, Au, etc.) systems have attracted increasing scientific interest as a consequence of the applications of such systems in the microelectronic industry [1,2]. Among these systems, Si/Al thin film couples are of special interest to study annealing induced transformations, because according to the thermodynamics for bulk materials, Si and Al do not form compounds and are rather immiscible [3].

For Si/Al bilayers, where both sublayers are crystalline, further indicated as c-Si/Al, it was found that the Al atoms diffuse through Si grain boundaries at a temperature as low as 300 °C [4]; at higher temperatures (400–560 °C), Si dissolves into Al followed by nucleation and growth of Si crystallites in the Al layer [5]. For Si/Al bilayers, where the Si layer is amorphous and the Al layer is crystalline, further indicated as a-Si/Al, various studies showed that the presence of Al layer lowers the crystallization temperature of a-Si significantly as compared to bulk a-Si [6]. In situ transmission

electron microscopy analysis of an a-Si/Al multilayer showed that, during annealing at 220 °C, c-Si nucleates within the Al layers and penetrates the Al as the c-Si grows [7]. Annealing an a-Si/Al bilayer in a dry N<sub>2</sub> ambient (350–500 °C) showed that c-Si nucleates at the Si/Al interface and grows further into the Al layer until, finally, a continuous c-Si film has formed [8].

In order to understand the transformations occurring in a-Si/Al thin film systems, in this study a systematic investigation on the microstructural (crystallite size, microstrain, texture and stress) evolution accompanying the annealing-induced transformations was performed, using in particular X-ray diffraction (XRD), Auger electron spectroscopy (AES) and focused-ion beam (FIB) imaging techniques. The research was focused on the interaction of a-Si and Al at low annealing temperature (250 °C) in vacuum. The occurring transformations were discussed with reference to the thermodynamic driving forces.

## 2. Experimental procedures

### 2.1. Specimen preparation and heat treatment

Commercially prepared, thermally oxidized, single crystal (510)-oriented Si wafer was used as substrate.

\*Corresponding author. Tel.: +49-711-689-3479; fax: +49-711-689-3312.

E-mail address: [j.y.wang@mf.mpg.de](mailto:j.y.wang@mf.mpg.de) (J.Y. Wang).

The thickness of the oxide layer was 50 nm. The Si(150 nm)/Al(50 nm) bilayer specimen was prepared by dc-magnetron sputter deposition in an ultra-high vacuum (UHV) system at a base pressure of  $10^{-7}$  Pa. The magnetron sputter apparatus has two exchangeable targets, enabling the preparation of the Si/Al bilayer specimen under vacuum in a single run. Before deposition, the substrate and the targets were cleaned by argon ion sputtering. Then, deposition of the Si/Al bilayer was carried out at room temperature under an Ar working pressure of  $4.0 \times 10^{-1}$  Pa. During sputtering, the substrate was rotated and its temperature increased from 20 to approximately 50 °C. The as-prepared Si/Al bilayer was annealed at 250 °C for 60 min in a vacuum of  $2.0 \times 10^{-4}$  Pa. Cooling of the annealed sample occurred under vacuum with a cooling rate of 2 °C/min.

## 2.2. Microstructural and compositional characterization

A Philips MRD diffractometer was employed to perform phase analysis and texture, residual stress, crystallite size and microstrain determinations. The diffractometer was equipped with a Eulerian cradle, a copper tube operating at 1.8 kW, X-ray lens and a secondary monochromator to select Cu  $K_{\alpha}$  radiation. To analyze the phases present in the as-prepared and annealed Si/Al bilayers, diffraction patterns were recorded by performing continuous  $\theta$ - $2\theta$  scanning from  $2\theta = 10^{\circ}$  to  $120^{\circ}$ , where  $2\theta$  is the diffraction angle. To study the texture of the Al layer, a  $\phi$  step scan from  $0^{\circ}$  to  $360^{\circ}$  for the  $\{111\}$  reflection of the Al layer was performed at specimen tilt angles  $\psi$  from  $0$  to  $90^{\circ}$ . For the determination of macrostress, crystallite size and microstrain,  $\theta$ - $2\theta$  step scans were performed for the Al  $\{111\}$  reflection at different  $\psi$  angles. The peak parameters (peak position, full width at half maximum and integral breadth) were then determined by fitting a Pearson VII function to the peaks in the measured diffraction patterns using Philips Profit 1.0c software.

The compositional characterization of the as-prepared and annealed Si/Al bilayers was performed using a JEOL 7830 scanning Auger microscope at a base pressure below  $8.0 \times 10^{-8}$  Pa. A static primary electron beam of 10 keV and 20 nA was used. The samples were sputtered using an ion gun with 1 keV Ar<sup>+</sup> ion beams. The ion incidence angle was approximately  $40^{\circ}$  with respect to the normal to the sample surface. The sputtered and analyzed areas were approximately  $1 \times 1$  mm and  $10 \times 10$   $\mu\text{m}$ , respectively. AES depth profiles of the samples were obtained by discontinuous ion sputtering mode. The Auger peak-to-peak heights of Al (1396 eV), Si (1621 eV) and O (507 eV) as a function of the sputtering time were quantified by applying the relative elemental sensitivity factors:  $S_{\text{Al}} = 0.23$  and  $S_{\text{Si}} = 0.16$  and  $S_{\text{O}} = 0.23$ , which were measured under the

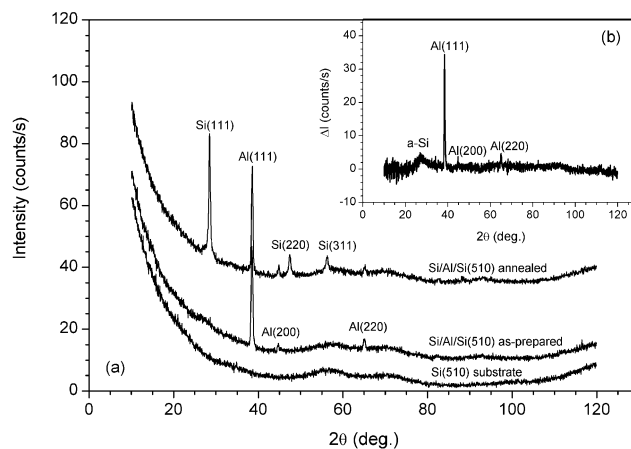


Fig. 1. (a) XRD patterns of the as-prepared and annealed Si(150 nm)/Al(50 nm)/Si(510) bilayer specimens as well as of the 'bare' thermally oxidized Si(510) substrate. Vertical offsets have been applied to the individual patterns to avoid overlap. (b) XRD pattern of the as-prepared Si/Al bilayer after subtraction of the XRD background as recorded from the 'bare' Si(510) substrate.

same experimental conditions by the present Auger microscope.

FIB imaging was performed using a FEI 200 XP FIB microscope. Elements Al and Si as well as (crystalline Al) grains with different crystallographic orientations show different (channeling) contrasts in the secondary electron images. A groove with the length of approximately 10  $\mu\text{m}$ , with depth and width of approximately 1  $\mu\text{m}$ , was cut on the surface of the Si/Al bilayer specimens by Ga<sup>+</sup> ion beam milling in order to observe the cross-sectional FIB images from the sidewall of the groove upon tilting the specimen.

## 3. Results

### 3.1. Phase analysis

The XRD patterns of the as-prepared and annealed Si(150 nm)/Al(50 nm)/Si(510) bilayer specimens as well as of the 'bare' thermally oxidized Si(510) substrate are shown in Fig. 1a. The XRD pattern of the as-prepared Si/Al bilayer after subtracting the XRD background as recorded from the thermally oxidized Si(510) substrate is shown in Fig. 1b. The Si sublayer in the as-prepared Si/Al bilayer is amorphous. This is evidenced by the broad scattering peak at approximately  $2\theta = 27^{\circ}$ , which is characteristic of a-Si (Fig. 1b). The Al sublayer exhibits a  $\{111\}$  fiber texture. After annealing, the a-Si layer had crystallized into polycrystalline Si. The crystalline Si shows a  $\{111\}$  texture, because the  $I_{220}/I_{111}$  and  $I_{311}/I_{111}$  intensity ratios of the crystallized c-Si are much smaller than those given by the standard values on the ICDD-JCPDS card (No. 26-1481).

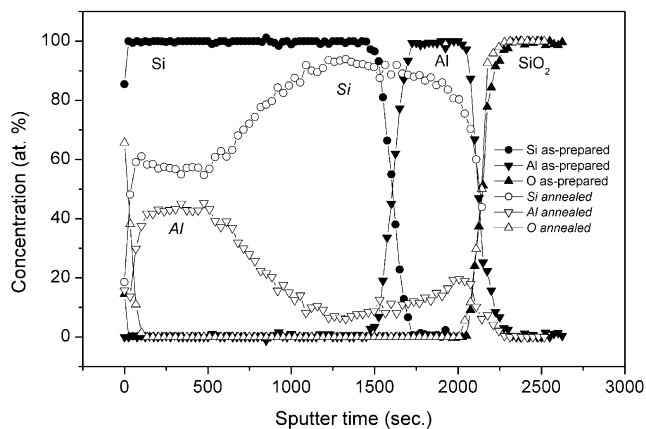


Fig. 2. AES depth-profiles of the as-prepared (filled points) and annealed (unfilled points) Si(150 nm)/Al(50 nm)/Si(510) bilayer specimens.

### 3.2. Compositional and morphological analyses

The AES depth profiles of the as-prepared and annealed Si(150 nm)/Al(50 nm)/SiO<sub>2</sub>(50 nm)/Si(510) bilayer specimens are shown in Fig. 2. The as-prepared Si/Al bilayer has a sharp interface between the outer a-Si and the inner crystalline Al layers. After annealing, most of the Si and Al layers have exchanged: most of the Al has moved to the surface and the Si has moved to the substrate. As follows from the O signal, no apparent compositional changes have occurred in the oxide (SiO<sub>2</sub>) layer of the Si(510) substrate upon annealing.

Cross-sectional FIB micrographs of the as-prepared and annealed Si/Al bilayer specimens, which were 45° tilted with respect to the specimen-surface normal, are shown in the middle parts of Fig. 3a,b. In case of the as-prepared bilayer, the Al layer and the Si layer can be

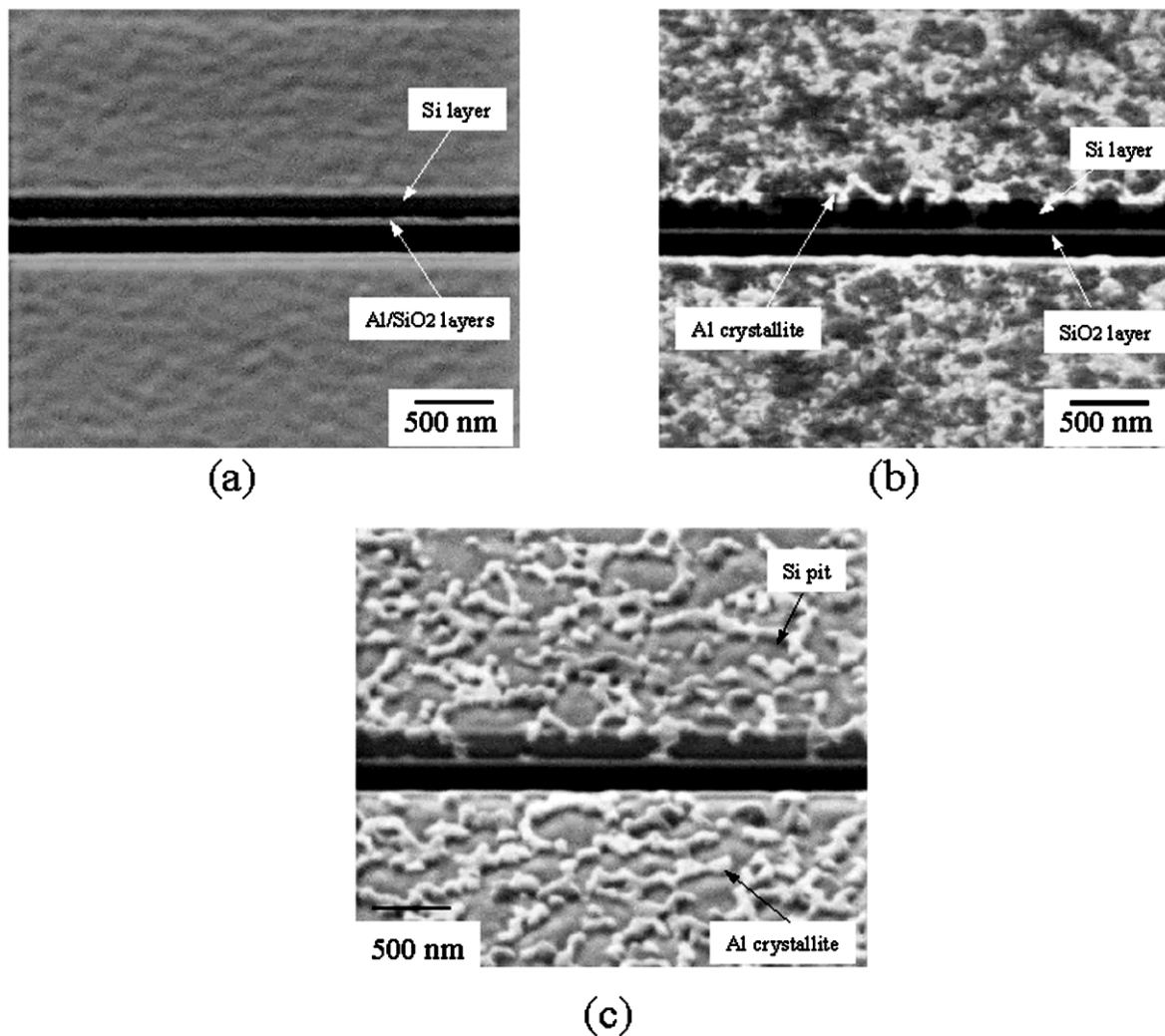


Fig. 3. FIB micrographs of the as-prepared (a) and annealed (b,c) Si/Al bilayers. (c) was taken at the same location as (b) but at a time 3 min later than (b) (i.e. 3 more min of Ga<sup>+</sup> ion sputtering). The middle parts of the micrographs are the cross-sectional FIB images, and the upper and the lower parts of the micrographs are the surface FIB images of the specimens.

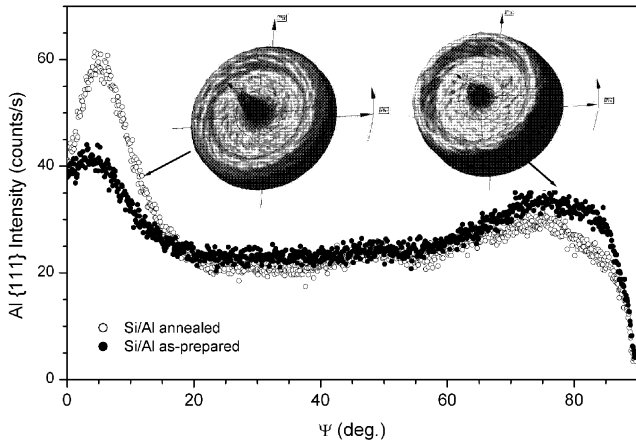


Fig. 4. The  $\psi$ -dependences of Al {111} peak intensities of the as-prepared (filled points) and the annealed (unfilled points) Si/Al bilayers. The insets represent the Al {111} pole figures for the as-prepared and annealed Si/Al bilayers.

clearly distinguished (Fig. 3a). After annealing, most of the Al layer had moved upwards and had formed a uniformly net-shaped structure (see the material of bright intensity in the upper and lower parts of the micrograph) on the surface; most of the Si layer has moved downwards to the SiO<sub>2</sub> layer on top of the substrate (see the material of dark intensity in the cross-sectional part of the micrograph). There are still some small Al grains left at the interface between the Si and the SiO<sub>2</sub> layers. The FIB observations agree with the above AES depth profiling results. In the FIB technique, a Ga<sup>+</sup> ion beam is used for generating the (secondary) electrons, which produce the image contrast. This ion beam brings about that surface atoms of the specimens are sputtered away during the observation. The sputtering rate of Si is larger than that of Al and, therefore, the Si present at the imaged surface will be sputtered away faster than the Al. The FIB image taken at the same location as in Fig. 3b but at a time approximately 3 min later, is shown in Fig. 3c. It can be concluded from Fig. 3b,c that upon annealing Al had arrived at the surface of the specimen uniformly, and enveloped Si grains.

### 3.3. Texture and residual stress analyses

The Al {111} pole figures of the as-prepared and annealed Si/Al bilayers are shown in Fig. 4 (see insets). Clearly, in both cases the Al sublayer exhibits a {111} fiber texture. The  $\psi$ -dependence's of the Al {111} peak intensities of the as-prepared and annealed Si/Al bilayers indicate that after annealing, the Al {111} texture had become stronger.

The Al {111} lattice strains,  $\varepsilon_{\{111\}}^{\text{Al}}$ , of the as-prepared (solid squares) and the annealed (unfilled squares) Si/Al bilayers, with reference to the lattice spacing,  $d_{\{111\}}^0$ ,

of standard Al powder ( $d_{\{111\}}^0 = 2.338 \text{ \AA}$ ), are shown as a function of  $\sin^2\psi$  in Fig. 5. For the cubic {111} fiber textured Al thin layer with a rotationally symmetric biaxial state of stress parallel to the surface, the lattice strain observed at specimen-tilt angle  $\psi$ ,  $\varepsilon_{\psi}$ , can be related to the stress parallel to the surface in the Al,  $\sigma_l$ , by [9]:

$$\varepsilon_{\psi} = \left( 2s_{12} + \frac{1}{2}s_{44}\sin^2\psi + \frac{2}{3}s_0 \right) \sigma_l \quad (1)$$

where  $s_0 = s_{11} - s_{12} - s_{44}/2$ , and  $s_{11}$ ,  $s_{12}$  and  $s_{44}$  are elastic compliances of single crystal Al, equal to 16.0 TPa<sup>-1</sup>, -5.8 TPa<sup>-1</sup> and 35.3 TPa<sup>-1</sup>, respectively [10]. Hence, a plot of  $\varepsilon_{\psi}$  vs.  $\sin^2\psi$  yields a straight line, and  $\sigma_l$  can be obtained from its slope. Thus it follows from Fig. 5 that the Al layer of the as-prepared specimen possesses a compressive stress parallel to the surface:  $\sigma_l = -139 \text{ MPa}$ , and that after annealing, the stress parallel to the surface of the Al has changed from compressive to tensile:  $\sigma_l = +182 \text{ MPa}$ .

### 3.4. Crystallite size and microstrain analyses

The measured diffraction-line profiles are the convolution of the structurally broadened profile of the sample with the instrumentally broadened profile [11]. The structurally broadened profile can originate from small crystallite size (often modeled with a Lorentzian broadening function) and/or the presence of microstrain (often modeled with a Gaussian broadening function). Here the instrumental broadening for the Al reflections was measured from a coarse-grained Al reference sample that did not exhibit significant structural broadening. On this basis, here the single line Voigt method was used to determine values for the crystallite size and the

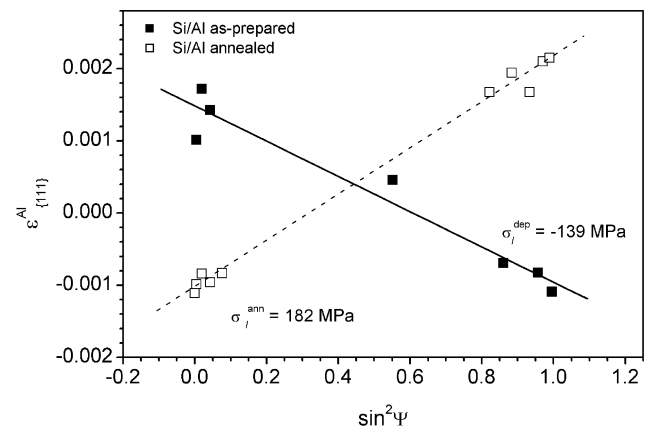


Fig. 5. The Al {111} lattice strain,  $\varepsilon_{\{111\}}^{\text{Al}}$ , of the as-prepared (filled squares) and annealed (unfilled squares) Si/Al bilayers, with reference to the lattice spacing,  $d_{\{111\}}^0$ , of standard Al powder, vs.  $\sin^2\psi$ .

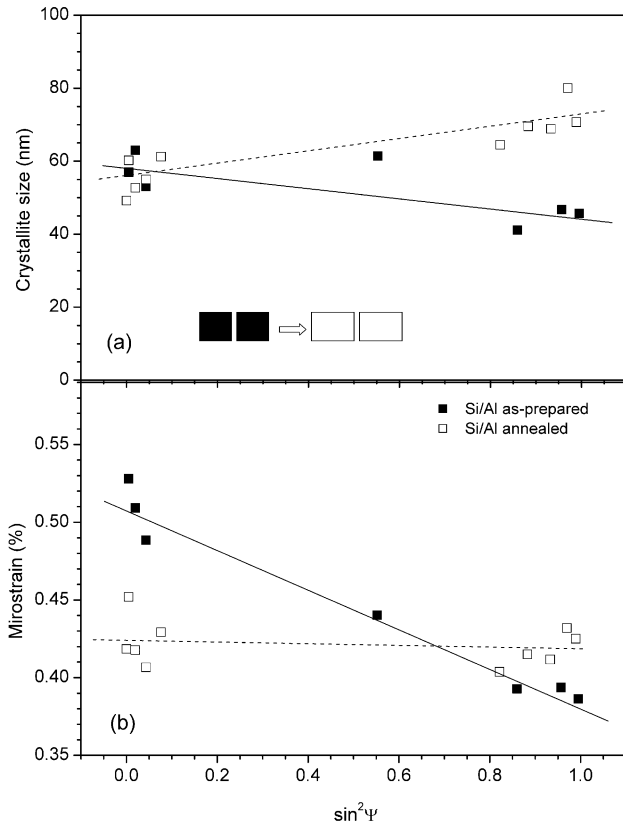


Fig. 6. The crystallite size (a) and microstrain (b) (for definitions, see Ref. [11]) vs.  $\sin^2\psi$  for the Al layer in the as-prepared (filled squares) and as-annealed (unfilled squares) Si/Al bilayers.

microstrain in the direction of the diffraction vector (for details, see Ref. [11]).

The crystallite (grain) size and microstrain of the Al (layer) in the as-prepared and annealed Si/Al bilayers are shown in Fig. 6a,b as a function of  $\sin^2\psi$  ( $\psi$  indicates the direction of the diffraction vector  $\mathbf{H}$ :  $\psi=0^\circ$ :  $\mathbf{H}$  is perpendicular to the surface;  $\psi=90^\circ$ :  $\mathbf{H}$  is parallel to the surface). It follows that for the as-prepared sample,

the Al-grain sizes along the layer surface ( $\psi=90^\circ$ ) and along the normal to the layer surface ( $\psi=0^\circ$ ) are nearly equal (approx. 50 nm), and of value comparable to the Al layer thickness. After annealing, the Al-grain size has remained about the same in the direction perpendicular to the surface and has increased laterally to approximately 70 nm (see the sketch in Fig. 6a). For the as-prepared Si/Al bilayer, the microstrain along the layer surface ( $\psi=90^\circ$ ) in the Al is smaller than perpendicular to the layer surface ( $\psi=0^\circ$ ). After annealing, the microstrain in Al perpendicular to the layer surface has relaxed and becomes an isotropic state of microstrain in the Al layer.

#### 4. Thermodynamic driving forces

Upon annealing an overall sublayer exchange occurs in the original Si(150 nm)/Al(50 nm) bilayer (see results in Section 3.2). To find the driving forces for this layer exchange, the Gibbs energy change upon transformation was calculated as described below.

A simplified, idealized representation of the transformation occurring in the initial Si(150 nm)/Al(50 nm) bilayer has been given in Fig. 7. At the start of the anneal at 250 °C (Fig. 7a), the Si layer is amorphous, and the Al layer is crystalline and subjected to a compressive macrostress and microstrain. At the end of the anneal at 250 °C, the Al and Si layers have exchanged their location, a-Si has crystallized into {111} textured polycrystalline Si, the grains of the Al layer have grown laterally, and the (macro)stress and the microstrain in the Al layer have been relaxed. The Gibbs energy change of the bilayer per unit area parallel to the surface,  $\Delta G$ , which has occurred at the end of annealing at 250 °C (Fig. 7b) as compared to the start of annealing at 250 °C (Fig. 7a), can be written as [12]:

$$\begin{aligned} \Delta G = & D_{\text{Si}}\Delta G_{\langle\text{Si}\rangle-\{\text{Si}\}} + D_{\text{Al}}\Delta G_{\text{Al}} + (\gamma_{\langle\text{Al}\rangle} - \gamma_{\{\text{Si}\}}) \\ & + (\gamma_{\langle\text{Al}\rangle-\langle\text{Si}\rangle} - \gamma_{\langle\text{Al}\rangle-\{\text{Si}\}}) \\ & + (\gamma_{\langle\text{Si}\rangle-\{\text{SiO}_2\}} - \gamma_{\langle\text{Al}\rangle-\{\text{SiO}_2\}}) \end{aligned} \quad (2)$$

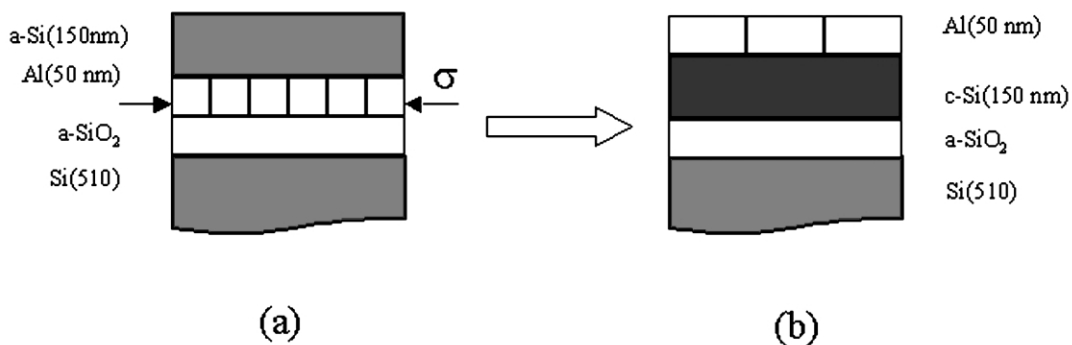


Fig. 7. Schematic representation of the layer exchange occurring upon annealing the Si(150 nm)/Al(50 nm) bilayer. At the beginning of annealing at 250 °C (a), the Si layer is amorphous, and the crystalline Al layer is subjected to a compressive stress and microstrain. At the end of annealing at 250 °C (b), the Al and Si layers have largely exchanged their locations, a-Si crystallized into {111} textured polycrystalline Si, the grain size of the Al has increased laterally and the macrostress and the microstrain of Al layer have relaxed.

The first term at the right-hand side of Eq. (2) is the Gibbs energy difference per unit area parallel to the surface between c-Si and a-Si;  $D_{\text{Si}}$  is the a-Si layer thickness, and  $\Delta G_{\langle \text{Si} \rangle - \langle \text{Si} \rangle}$  is the Gibbs energy difference between c-Si and a-Si at 250 °C per unit volume, which can be estimated from the crystallization enthalpy of a-Si [13]. The first term is thus estimated to be  $-125.95 \text{ J/m}^2$  [14].

The second term at the right-hand side of Eq. (2) is the Gibbs energy change per unit area parallel to the surface between the annealed Al layer and the as-prepared Al layer;  $D_{\text{Al}}$  is the Al layer thickness, and  $\Delta G_{\text{Al}}$  is the Gibbs energy difference between the annealed and unannealed Al layers per unit volume. This last term includes two components: energy differences due to Al-grain growth and release of (macro)stress and microstrain energy. The energy change by Al-grain growth can be calculated from the grain-boundary energy and the reduction of the grain-boundary area; it is estimated at  $-0.28 \text{ J/m}^2$  [14]. The released macrostress and microstrain energy is estimated on the basis of elastic theory to be  $-0.25 \text{ J/m}^2$  [14].

The third term represents the difference in surface energy between crystalline Al (c-Al,  $\gamma_{\langle \text{Al} \rangle}$ ) and a-Si ( $\gamma_{\langle \text{Si} \rangle}$ ). This term is calculated to be  $0.15 \text{ J/m}^2$  [14]. The fourth term is the interface-energy difference between c-Al/c-Si ( $\gamma_{\langle \text{Al} \rangle - \langle \text{Si} \rangle}$ ) and c-Al/a-Si ( $\gamma_{\langle \text{Al} \rangle - \langle \text{Si} \rangle}$ ). It is calculated to be  $0.22 \text{ J/m}^2$  [14]. The 5th term is the interface-energy difference between c-Si/a-SiO<sub>2</sub> ( $\gamma_{\langle \text{Al} \rangle - \langle \text{SiO}_2 \rangle}$ ) and c-Al/a-SiO<sub>2</sub> ( $\gamma_{\langle \text{Al} \rangle - \langle \text{SiO}_2 \rangle}$ ). This term can be neglected, as compared to the other terms at the right-hand side of Eq. (2), since the solid ('crystalline')/liquid ('amorphous') interface energy is one order of magnitude smaller than that of the solid/solid interface.

The largest contribution to the driving force for the transformation is due to the crystallization of the amorphous Si. However, this driving force contribution cannot explain why layer exchange occurs. The above calculations show that the changes in surface and interface energies also cannot promote the layer exchange. Hence, one is led to the conclusion that the layer exchange may be due to the relaxation of the elastic energy associated with the macrostress and the microstrain: due to the drastic atomic rearrangement within the bilayer, by the layer exchange, the misfit experienced in the initial, unannealed condition can be relieved. Indeed, the above calculation suggests that the unfavorable changes in surface and interface energies are over-compensated by the favorable changes in elastic energy.

An alternative explanation for the layer exchange may be of kinetic origin (see Ref. [14]).

It is remarked that the tensile stress parallel to the surface of the Al layer as observed after annealing can be ascribed to the thermal stress induced by the cooling after the annealing [14]. Hence, the compressive macrostress in the Al completely relaxes indeed upon annealing.

## 5. Conclusion

Upon annealing of an a-Si/Al bilayer at 250 °C the Si and Al largely exchanged their positions. The initially surface adjacent amorphous Si moved in the direction of the substrate and crystallized; the Al moved upwards in association with release of macrostress and microstrain. The largest gain in energy upon transformation is due to the crystallization of the amorphous Si. The only identifiable driving force for the layer exchange appears to be the release of elastic energy upon the rearrangement of the Si and Al phases in the layer.

## Acknowledgments

We thank Mr F. Thiele for sputter deposition of the layers and Dr C. Volkert for assistance with FIB imaging.

## References

- [1] S.R. Herd, P. Chaudhari, M.H. Brodsky, *J. Non-Cryst. Solids* 7 (1972) 309.
- [2] G. Ottaviani, D. Sigurd, V. Marrello, J.W. Mayer, J.O. McCaldin, *J. Appl. Phys.* 45 (1974) 1730.
- [3] J.L. Murray, A.J. McAlister, *Bull. Alloy Phase Diagrams* 5 (1984) 74.
- [4] K. Nakamura, M. Kamoshida, *J. Appl. Phys.* 48 (1977) 5349.
- [5] K. Nakamura, M-A. Nicolet, J.W. Mayer, R.J. Blattner, C.A. Evans, *J. Appl. Phys.* 46 (1975) 4678.
- [6] J.R. Bosnell, U.C. Voisey, *Thin Solid Films* 6 (1970) 161.
- [7] J.K. Toyohiko, S. Robert, *Phil. Mag. Part B* 66 (1992) 749.
- [8] O. Nast, S.R. Wenham, *J. Appl. Phys.* 88 (2000) 124.
- [9] A.C. Vermeulen, R. Delhez, Th H. de Keijser, E.J. Mittemeijer, *J. Appl. Phys.* 77 (1995) 5026.
- [10] E.A. Brandes, G.B. Brook, *Smithells Metals Reference Book*, 7th ed, Butterworth-Heinemann Ltd, Oxford, 1992, pp. 15–25.
- [11] R. Delhez, Th H. de Keijser, E.J. Mittemeijer, *Fres. Z. Anal. Chem.* 312 (1982) 1.
- [12] E.P. Donovan, F. Spaepen, D. Turbull, J.M. Poate, D.C. Jacobson, *J. Appl. Phys.* 57 (1985) 1795.
- [13] R. Benedictus, A. Böttger, E.J. Mittemeijer, *Phys. Rev. Part B* 54 (1996) 9109.
- [14] Y.H. Zhao, J.Y. Wang, E.J. Mittemeijer, to be submitted.